Inorganic Chemistry

Article

pubs.acs.org/IC

Shedding Light on the Single-Molecule Magnet Behavior of Mononuclear Dy^{III} Complexes

Daniel Aravena and Eliseo Ruiz*

Departament de Química Inorgànica and Institut de Recerca de Química Teòrica i Computacional, Universitat de Barcelona, Diagonal 645, E-08028 Barcelona, Spain

Supporting Information

ABSTRACT: General requirements for obtaining Dy^{III} single-molecule magnets (SMM) were studied by CASSCF+RASSI calculations on both real and model systems. A set of 20 Dy^{III} complexes was considered using their X-ray crystal structure for our calculations. Theoretical results were compared with their experimental slow relaxation data, and general conclusions about the calculated key parameters related with SMM behavior are presented. The effect of the coordination geometry and nature of ligands is discussed based on calculations on real and model systems. We found two different patterns to exhibit SMM behavior: the first one leads to the largest axial anisotropy in complexes showing heterolepticity of the ligand environment (more important than symmetric requirements), while the second one corresponds to sandwich-shaped complexes with a smaller anisotropy. Thus, most existing mononuclear zero-field SMMs adopting a heteroleptic coordination mode mixing neutral and anionic ligands present the same pattern in the electrostatic potential induced by their ligands, with a lower potential island related to the presence of neutral ligands inside a high potential background related with anionic groups. The existence of different electrostatic regions caused by the ligands induces a preferential orientation to reduce the electron repulsion for the electron density of the Dy^{III} cations, resulting in the magnetic anisotropy.

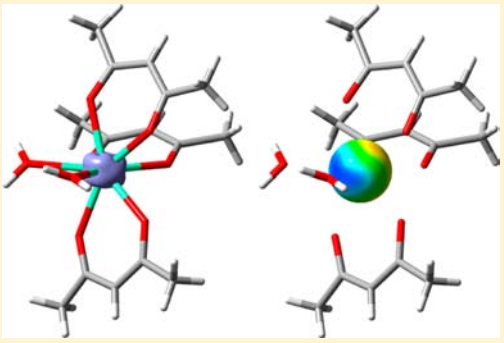

INTRODUCTION

Considerable effort has been made to produce molecular materials that could behave as small nanomagnets (single-molecule magnets, SMMs). SMM behavior was detected for the first time at a low temperature in an $[Mn_{12}O_{12}(CH_3COO)_{16}(H_2O)_4]$ complex usually known as Mn_{12} ($8Mn^{III}4Mn^{IV}$).[1,2] The first systems were polynuclear transition metal complexes that exhibit slow relaxation of their magnetization, which is essentially controlled by an energy barrier that may fix the direction of spin. That spin direction may flip (relaxation process) due to thermal crossing of the barrier or tunneling, both from the ground state, or the process may be thermally assisted through low-lying excited states. SMM systems have two specific characteristics that have been well described in the past: steps in their hysteresis loops due to tunneling effects and frequency dependence of the imaginary part of the magnetic susceptibility under ac magnetic fields.[3,4] From a practical point of view, it is more common to employ susceptibility measurements under ac fields to probe SMM properties.

Many research groups have been searching for new high-nuclearity systems[5,6] with large barriers in the hope of devising high-temperature applications (since current SMMs normally present slow relaxation of their magnetization only below 10 K). However, in 2003, Ishikawa and co-workers[7] presented a mononuclear complex $[TbPc_2]^-$ containing only one Tb^{III} cation that exhibits slow magnetization relaxation together with a huge anisotropic barrier. Since 2008, several mononuclear lanthanide complexes, especially those containing Dy^{III} cations, some actinide species, with U^{III} and Np^{III} cations,[8−10] and also a number of mononuclear first-row transition metal complexes[11−16] have shown similar SMM behavior and been called single-ion magnets; we prefer the term mononuclear single-molecule magnets. Taking into account the number of reported SMMs, Dy^{III} ($^6H_{15/2}$ ground state) is the most prolific cation, probably due to its high (and half-integer) $J = 15/2$ value for the ground state.[17] As previously noted, complexes with half-integer J values and a Kramers doublet as their ground state are better candidates to exhibit SMM behavior,[18] but it must also kept in mind that such behavior can also be found in integer J complexes usually related with high-symmetric metal environments, i.e., Tb^{III} double-decker systems. In addition to SMMs, a number of compounds exhibit SMM features only in the presence of a dc magnetic field. The effect is related with suppression of tunneling effects between low-energy levels, and such systems are usually named field-induced single-molecule magnets, in contrast with those that show the same behavior without an external dc field (zero-field single-molecule magnets).

Despite many mononuclear SMM Dy^{III} complexes being studied, there is a lack of a comparative theoretical study of the different magnetic behaviors found in such family of systems.

Received: September 18, 2013
Published: November 15, 2013

Table 1. Mononuclear Dy^{III} Complexes Studied (see full names in the Supporting Information) Indicating Whether Each Is a Zero-Field SMM (complexes 1−11), a Field-Induced SMM (complexes 12−21), or Not an SMM (complexes 22−24), together with the Experimental Magnetic Anisotropy Barrier (U_{eff}, in cm^{-1}) and the Values Calculated at the CASSCF+RASSI Level for the First Excitation Energy After SOC Inclusion (U_{calcd}, in cm^{-1}), the g Components, and $g_{xy} = (g_x^2 + g_y^2)^{1/2}$

	CSD REFCODE	SMM $H = 0$	SMM $H \neq 0$	U_{eff}	U_{calcd}	g_z	g_y	g_x	g_{xy}	ref
1	DARTOH	yes		94	120.4	19.237	0.014	0.004	0.015	30
2	DARTUN	yes		130	146.2	19.368	0.009	0.005	0.010	30
3	GUYRAU	yes		45.9	151.9	19.457	0.007	0.005	0.009	31
4	ISEBIS	yes		44.4	135.8	19.389	0.007	0.004	0.008	32
5	MAVQIL	yes		16						33
6	UCEZUZ	yes		40	142.6	19.595	0.006	0.003	0.007	34
7	UCIBAL	yes		59	126.3	19.511	0.009	0.005	0.010	34
8	WUQNOM	yes		37.8	67.2	19.243	0.326	0.158	0.362	35
9	$Dy[COT"]_2^{-}$ [b]	yes		17	45.6	16.896	0.071	0.024	0.075	36
10	BAJSIQ	yes		12	36.3	15.952	0.183	0.140	0.230	37
11	$Dy(paaH)_2(H_2O)_4$ [b]	yes		124	243.5	19.652	0.001	0.001	0.001	23
12	$Dy(paaH)_2(NO3)_2(MeOH)$ [b]	no	2000 Oe	44	111.0	19.592	0.017	0.013	0.021	23
13	HEBYEU	no	1000 Oe	16	188.9	19.482	0.051	0.027	0.058	38
14	ITEDER01	no	2000 Oe	21.1	93.0	19.258	0.067	0.023	0.071	39
15	MAVQOR	no	2000 Oe	30						33
16	MAVQUX	no	2000 Oe	40						33
17	NEHBUZ	no	1000 Oe	22.2	80.4	18.988	0.654	0.221	0.690	40
18	RAXZIB	no	1000 Oe [a]	19.7	77.3	16.086	0.662	0.625	0.910	41
19	RAXZOH	no	1000 Oe [a]	24.0	75.3	16.853	0.571	0.488	0.751	41
20	TAKQIH	no	2000 Oe	28.5	109.1	19.685	0.025	0.011	0.027	42
21	YACYOS	no	1000 Oe [a]	17	58.7	19.684	0.027	0.019	0.033	43
22	ITEDER	no			40.8	17.932	0.509	0.223	0.556	39
23	MANHOY01	no			106.6	18.951	0.477	0.211	0.522	32
24	OYUTUY	no								44

[a] Diluted sample. [b] Not in CSD database.

Trends in SMM properties are difficult to extract in lanthanide complexes because their f-shell interelectronic repulsion terms are predominant, the ground state wave function has a large multireference character, and there are very important spin−orbit effects. These facts prevent straightforward use of molecular orbitals to understand the magnetic properties as is possible in mononuclear first-row transition metal complexes, where a simple orbital picture can explain the large anisotropy present in some systems.[15,19−21] Some qualitative attempts have been made using the simple criterion of the reduction of the electronic repulsion; in that way, analysis of the shape (prolate and oblate) of the electron density of the ground state of the lanthanide together with the spatial distribution of the ligands allows us to make some predictions.[22] For instance, Chilton et al. were successful to synthesize two Dy^{III} complexes showing SMM behavior corroborating the predictions of the prolate/oblate concept to determine the magnetization axis.[23] Furthermore, some crystal-field models have been employed to predict the SMM of mononuclear lanthanide complexes.[24,25] However, such magnetic properties are extremely sensitive to small changes in the structure of the complexes, as shown by the experimental and theoretical study of the strong influence on SMM behavior of the rotation of the hydrogen atoms in the water ligands in mononuclear Dy^{III} complexes.[26] Simple qualitative models are not therefore suitable for seeking explanations of important variations in the magnetic properties for complexes in which the symmetry and ligands remain almost unchanged.

In contrast, high-level calculations based on the CASSCF +RASSI methodology have successfully been employed to study the magnetic properties of mononuclear SMM Dy^{III} complexes,[27−29] allowing inclusion of spin−orbit effects (RASSI) in a multireference wave function (CASSCF). The very ionic nature of the metal−ligand bonds in lanthanides due to the very localized 4f orbitals can be accurately described without including dynamic correlation. However, such studies have usually focused on individual complexes, which do not favor extraction of more general conclusions regarding a broader set of molecules. Hence, our main goal here is to gain an understanding of, and thereby rationalize, magnetic behavior in the family of mononuclear Dy^{III} complexes using theoretical methods based on CASSCF+RASSI calculations. In the first part of this study, we consider the potential of CASSCF+RASSI calculations to provide useful information about the experimental magnetic behavior of a set of previously published Dy^{III} complexes. From a comparison between experimental ac susceptibility data and calculated parameters (g tensor components and state energies), we discuss the performance of the methodology and the necessary conditions for the presence (or suppression) of SMM behavior. In the second part of the study, we explore the influence of the geometry of the ligand environment through the electrostatic potential generated by the ligands on SMM properties, employing both CASSCF+RASSI calculations and structural analysis of the coordination sphere. Existing models are discussed, and some general conclusions about the most appropriate conditions for obtaining Dy^{III} SMMs are proposed.

RESULTS AND DISCUSSION

Multiconfigurational Calculations and Correlations with Experimental Data. Table 1 shows experimental information on the Dy^{III} mononuclear complexes considered.

dx.doi.org/10.1021/ic402367c | Inorg. Chem. 2013, 52, 13770−13778

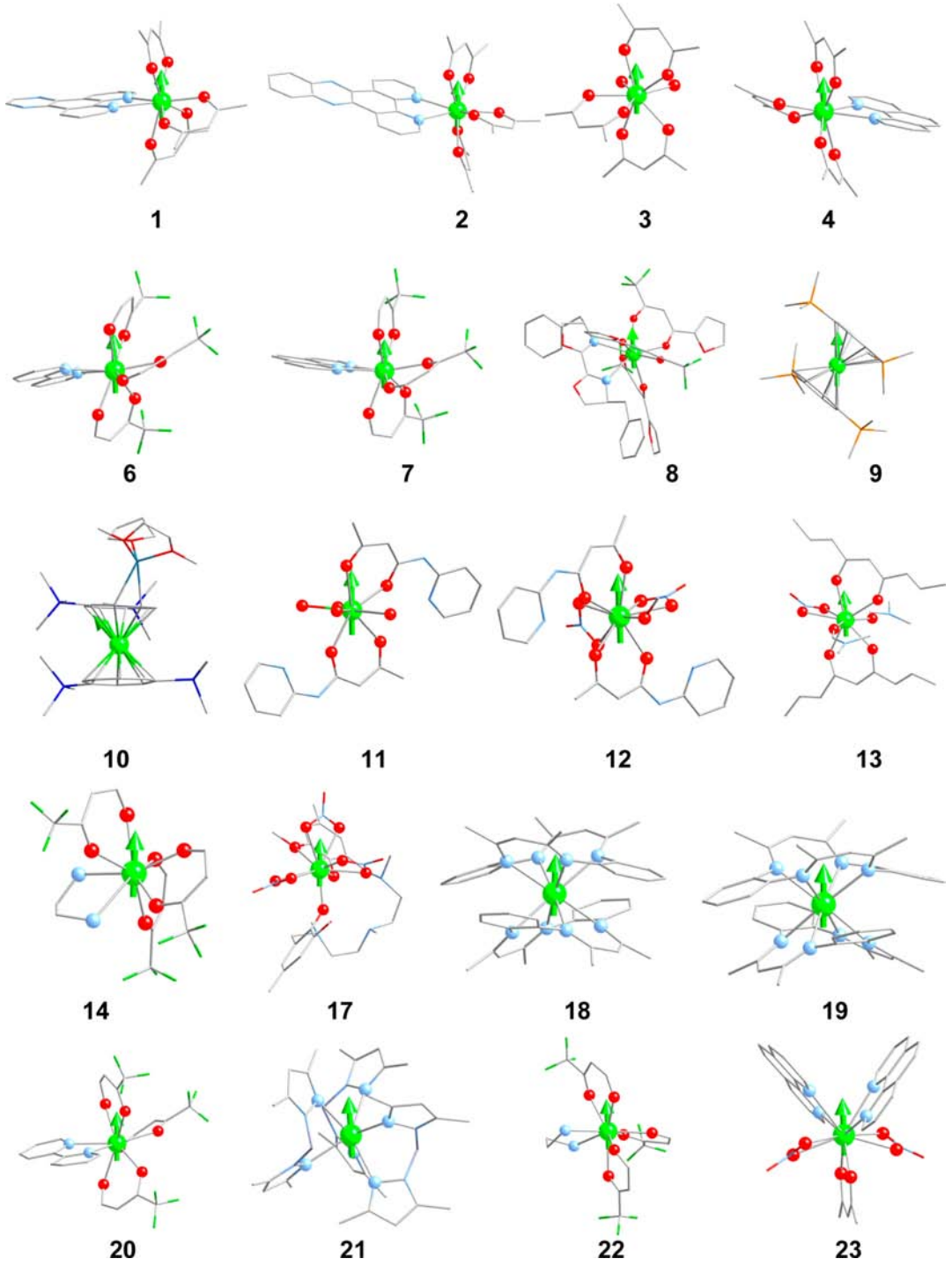

Figure 1. Calculated Dy^{III} complexes (see full names in Supporting Information) showing the direction of the magnetization easy axis. Dy, O, and N atoms (first coordination sphere) are green, red, and blue spheres, respectively.

Using SMM behavior as a criterion, we can classify the complexes into three groups: (i) those showing zero-field SMM (determination of a maximum of the χ'' from ac measurements); (ii) systems that, under a static field (suppression of tunneling effects), show field-induced SMM behavior; and (iii) complexes that even in the presence of static fields do not show SMM behavior. It is worth noting that in some cases the sample was diluted to diminish magnetic dipolar interactions between neighboring complexes and thus facilitate determination of the reversal of the magnetization barrier.

From the calculated results, we can see that the ground state is always markedly axial, with g_z values ranging from 16 to almost 20. The magnetic anisotropy barrier was estimated assuming that relaxation will pass through the first excited state. Thus, the U_{calcd} values correspond to the calculated first excitation energy after inclusion of the spin−orbit coupling. A comparison between the experimentally estimated U_{eff} energy barrier and the corresponding calculated U_{calcd} value shows that there is no proper correlation between the two. The origin of this discrepancy may be related with the presence of additional relaxation mechanisms (for example, tunneling in the ground

dx.doi.org/10.1021/ic402367c | *Inorg. Chem.* 2013, 52, 13770−13778

Table 2. Mononuclear Dy^{III} Complexes for Which the Calculations Were Performed, Indicating Whether Each Is a Zero-Field SMM, a Field-Induced SMM, or Not an SMM, Calculated CASSCF (spin-free) First and Second Excitation Energies (E_1 and E_2, in cm^{-1}), and $(E_2 - E_1)/E_1$ Parameter

	CSD REFCODE	SMM $H = 0$	SMM $H \neq 0$	E_1	E_2	$(E_2 - E_1)/E_1$
1	DARTOH	yes		3.9	157.1	39.3
2	DARTUN	yes		7.4	195.1	25.4
3	GUYRAU	yes		5.1	195.0	37.2
4	ISEBIS	yes		7.3	189.8	25.0
6	UCEZUZ	yes		8.6	139.0	15.2
7	UCIBAL	yes		11.0	141.7	11.9
8	WUQNOM	yes		41.0	98.5	1.4
9	$Dy[COT'']_2^-$	yes		2.0	39.4	18.7
10	BAJSIQ	yes		9.4	46.0	3.9
11	$Dy(paaH^*)_2(H_2O)_4$	yes		8.1	356.5	44.0
12	$Dy(paaH^*)_2(NO3)_2(MeOH)$	no	2000 Oe	28.9	140.5	4.9
13	HEBYEU	no	1000 Oe	14.3	248.6	16.4
14	ITEDER01	no	2000 Oe	26.2	136.6	4.2
17	NEHBUZ	no	1000 Oe*	77.5	138.7	0.8
18	RAXZIB	no	1000 Oe*	12.8	22.8	0.8
19	RAXZOH	no	1000 Oe*	9.6	10.3	0.1
20	TAKQIH	no	2000 Oe	7.7	88.8	10.5
21	YACYOS	no	1000 Oe*	2.2	69.9	30.8
22	ITEDER	no		45.1	109.2	1.4
23	MANHOY01	no		39.6	156.8	3.0

state or induced by dipolar coupling with neighboring molecules or vibronic coupling)[13,45] that are important for the experimental U_{eff} values but were not considered in the U_{calcd} values. The effect of these additional demagnetization pathways can be clearly observed in field-induced SMMs, where inclusion of a small dc field suppresses tunneling of the ground state to some extent and allows determination of a relaxation barrier that is not observed at zero field. In this study of Dy^{III} complexes, we focus on tunneling within the Kramers doublet ground state. We consider the magnitudes of the g_x and g_y components that describe this ground state as parameters to characterize the magnitude of the tunneling, at least qualitatively. These terms mix the states of the ground doublet, even if the magnetic field is aligned with the main anisotropy axis (they do not commute with the Zeeman operator when the field is aligned with the main anisotropy axis); the role of transverse anisotropy has been already related with the SMM behavior.[46,47] It can be observed that complexes that present zero-field SMM behavior (see Table 1) present low g_{xy} values (<0.015), with the exception of the **9** and **10** sandwich complexes, which present very low experimental thermal barriers that were highly sensitive to an external dc field, highlighting the considerable contribution of ground state tunneling to magnetic relaxation in these compounds.[37] Field-induced SMMs span a broad range of values (0.027–0.910); finally, complexes that do not show SMM behavior show high g_{xy} (>0.5). An exception to this trend is the WUQNOM complex,[35] which is a zero-field SMM and presents a high g_{xy} value (0.362). However, this compound is also ferroelectric at room temperature; the structural changes associated with ferroelectric behavior could make the room-temperature X-ray structure very different from the geometry at low temperature (that it is unavailable), where ac susceptibility measurements are performed. It is interesting to compare ITEDER01 (field-induced SMM) and ITEDER (no SMM) because they are polymorphs of the same complex with different coordination geometries, originally described as a distorted bicapped triangular prism and a distorted dodecahedron, respectively.[39] It can be observed that the g factors calculated for ITEDER01 are much more axial than those of ITEDER, in agreement with the experimental magnetic properties of these systems. Another important point is the broad range of g_{xy} values for field-induced SMMs. We believe that it is related to the fuzziness of our definition of this group, given that different experiments were not performed under the same conditions, especially with respect to external magnetic fields and dilution conditions.

The calculated g factors of the ground state and first excitation energies after inclusion of spin–orbit effects (U_{calcd}, usually considered as the spin relaxation barrier) are also included in Table 1. Some of the experimental compounds were not calculated, and others were truncated due to the large number of atoms, which prevented calculations at the CASSCF level with reasonable computational facilities (see calculated complexes in Figure 1 and the Computational Details section). As seen previously, the g_x and g_y values (or g_{xy}) calculated at the CASSCF+RASSI level can help to classify the Dy^{III} complexes with respect to their SMM properties. However, it is not easy to make an a priori prediction of their magnitudes. In order to extract more information, we can analyze what the requirements of the spin-free states are (before applying RASSI to add spin–orbit effects) for the g_x and g_y values to be small. We find that to obtain a strongly axial ground state after inclusion of spin–orbit coupling it is necessary to have a very low spin-free first excited state (E_1 energy), while the second one (E_2 energy) needs to be as high as possible (see below). In such cases, the final ground doublet will mainly be composed of the ground and first excited spin-free states after the mixing induced by the spin–orbit operator.

We propose as a figure of merit the $(E_2 - E_1)/E_1$ parameter given in Table 2: high calculated $(E_2 - E_1)/E_1$ parameters should correlate with more axial g tensors and, consequently, with SMM behavior. From Table 2, two different patterns can be observed: (i) systems with small E_1 and large E_2 values show zero-field SMM behavior (with the exceptions of WUQNOM

dx.doi.org/10.1021/ic402367c | Inorg. Chem. 2013, 52, 13770–13778

and BAJSIQ complexes, mentioned above), and (ii) systems with small E_1 and relatively small E_2 values are usually field-induced SMM (sandwich complexes **18** and **19** and complex **20**). In order to make predictions, we would need to be able to estimate the E_1 and E_2 excitation energy values for new complexes. As mentioned in the Introduction, in lanthanide systems it is not easy to translate the splitting of the f orbitals due to ligand effects into excitation energies, due to the large differences in the interelectronic repulsion values in the f orbitals and large multiconfigurational character of the ground state. The small splitting (around 1000 cm^{-1}) of the ground ^6H spin-free term at the CASSCF level and strong configuration mixing of these low-energy wave functions found in all complexes illustrate the need of a multiconfigurational treatment in order to describe the electronic structure of Dy^{III} complexes.

Analysis of the Coordination Symmetry of the Mononuclear Dy^{III} Complexes. In order to establish some correlations between magnetic properties and the symmetry of the Dy^{III} coordination spheres, we employed continuous symmetry measurements (Shape code)[48,49] that allowed us to quantify the degree of distortion of the coordination sphere of real complexes (S value equals 0, corresponds to the perfect polyhedron) using three 8-coordination nondistorted polyhedra (SAPR, square antiprism; TDD, dodecahedron; and cube, see Figure 2 and Table S1, Supporting Information).

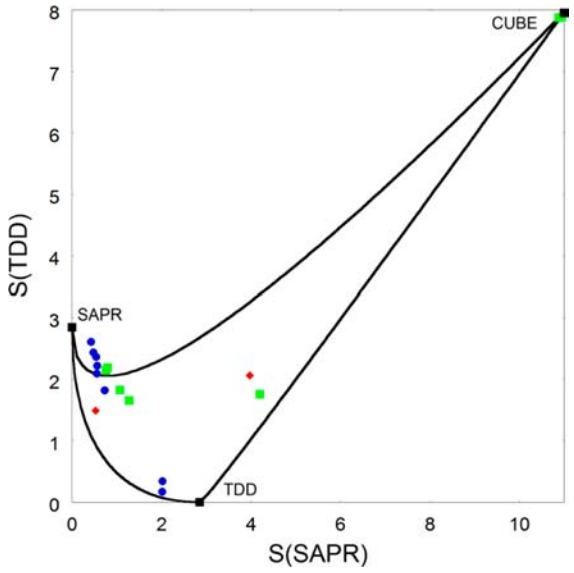

Figure 2. Continuous symmetry map (SAPR, square antiprism; TDD, dodecahedron) for the family of studied Dy^{III} complexes studied (Table 1). Blue circles, zero-field SMMs; green squares, field-induced SMMs; red diamonds, no SMM behavior.

From that figure we can extract some conclusions: (i) most of the systems adopt a conformation close to a square antiprism, which can present SMM properties but does not in all cases; (ii) systems with cube symmetry do not present SMM behavior; and (iii) the two cases with symmetry close to a dodecahedron structure (GUYRAU, **3**, and Dy-(paaH*)$_2$(H$_2$O)$_4$, **11**) are zero-field SMM.

At this point, it is possible to check whether the symmetry of the structure is really the key parameter that dictates SMM behavior in the complexes studied. To that end we repeated the calculations for the Dy^{III} complexes, this time replacing the O and N ligands by water and ammonia molecules, respectively, while maintaining the position of the coordinated metal atoms present in the coordination sphere. Results are shown in Table S2, Supporting Information. There are large variations in the calculated g components; the model structures have larger g_x and g_y values than the real complexes, except for the case of **14**. Thus, changes in the nature of the ligand can considerably modify the magnetic properties and mean that exclusive use of symmetry criteria is unsuitable for predicting such properties. This result agrees, for instance, with the finding that the magnetization direction strongly depends on the rotation of the hydrogen atoms of a water ligand, as revealed by Sessoli and co-workers[26] (we will discuss this system later).

Role of the Electrostatic Potential Caused by the Ligands in the Magnetic Anisotropy. Besides the nature of the ligands, the charge of the coordinated molecules could also have a strong effect on the magnetic properties of Dy^{III} complexes, as that factor should affect the shape of the electrostatic potential that will interact with the f electrons of the Dy^{III} ion. Studying the electrostatic potential will allow us to analyze how the electron density of the Dy^{III} centers can be arranged to reduce the electron repulsion. This is a similar idea to that already considered by Rinehart et al. with the prolate/oblate model.[22] In order to better represent the anisotropy of the f electron density of the Dy^{III} centers ($4f^9$), we only considered the two beta electrons (because the other seven alpha $4f^7$ electrons produce an isotropic spherical distribution). In the rest of this paper, we will use such partial electron density calculated at spin-free CASSCF states (corresponding to the two electrons of the Dy^{III} centers) as magnitude to discuss the magnetic anisotropy. The total electron density of the nine 4f electrons will be also anisotropic if the two beta electrons present a nonspherical density distribution; however, the isotropic density of the seven alpha electrons make the anisotropic distribution harder to visualize; thus, we choose to illustrate only the two beta electrons. Mixing of such spin-free states induced by the spin−orbit coupling will result in the ground state of the system that will determine the magnetic properties. Thus, taking into account the energy differences between the ground and the excited states (Table 2), we can make a qualitative estimation of the shape corresponding to electron density that causes the magnetic anisotropy. It is worth mentioning that the anisotropic shape of the electron density of this final ground state including spin−orbit coupling cannot be easily visualized because there is not distinction between alpha and beta electrons; the whole density of the nine f electrons should be plotted.

For a zero-field SMM such as complex **3** (see Figure S1, Supporting Information), we obtain an axially compressed shape equivalent to a disc ($^6H_{15/2}$ m_J = 15/2 ground state of the Dy^{III} center, oblate in terms of the reference 22) with its main magnetic anisotropy axis perpendicular to the beta electron density plane. In Figure S1, Supporting Information, we represented such beta electron density for the first three spin-free states. We can now understand better the previous statement that the magnetic anisotropy will be larger if E_1 is small and E_2 is large (the energy differences between the ground state and the first and second excited states, respectively). In such cases, the spin−orbit coupling mainly has the effect of mixing the first two states with similar electron distributions (see Figure S1, Supporting Information); thus, the beta electron density of the spin−orbit ground state is mostly a combination of two electron distributions that are similar with

dx.doi.org/10.1021/ic402367c | Inorg. Chem. 2013, 52, 13770−13778

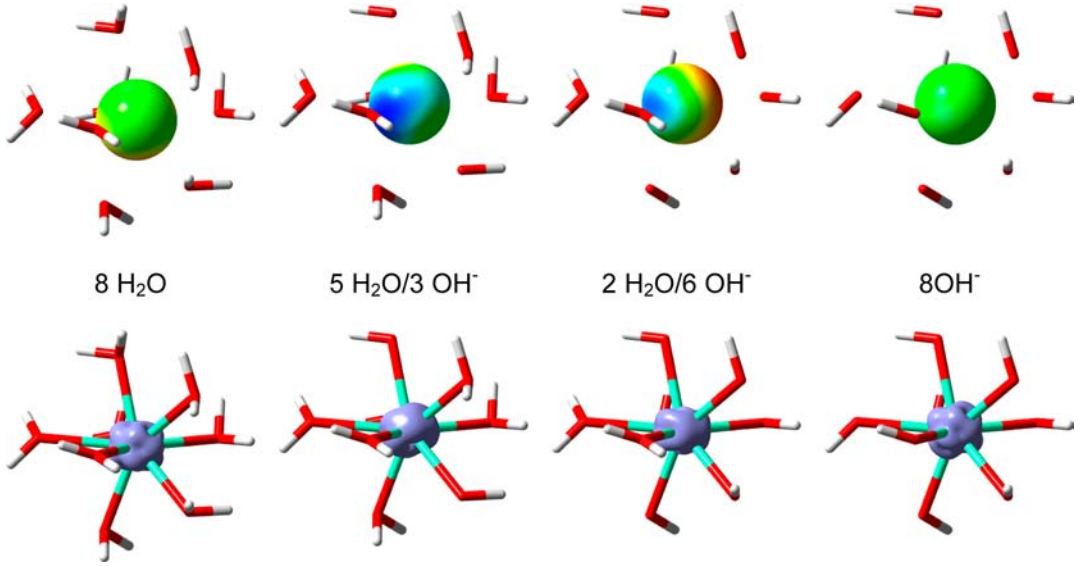

Figure 3. (Top) Electrostatic potential projection (a range of 0.09 au was adopted with the limit values in red and blue to compare systems with different electrostatic potential values) on a sphere of 1 Å of radius centered in the Dy position caused by the ligands fixed for the truncated models of **3**. (Bottom) Isosurface of the calculated beta electron density of the complexes calculated as the difference between the total density and the spin density of the seven alpha active electrons.

little contribution from the third state, whose different shape (see Figure S1, Supporting Information) would reduce the anisotropy.

In order to study the influence of the charge of the ligands, we constructed additional model structures for complex **3**: one with all ligands replaced by hydroxide ions (8 OH^- model in Table S3, Supporting Information); another with 5 water molecules and 3 OH^- groups ($5H_2O/3OH^-$); and a $2H_2O/6OH^-$ model. We found that the 2 homoleptic models (only water or OH^- ligands) presented g_x and g_y values that were too high compared to the full complex calculations and therefore not appropriate to be SMMs (see isotropic electron densities for these two homoleptic models in Figure S1, Supporting Information). In contrast, models combining H_2O and OH^- ligands give more axial g factors similar to those obtained for complex **3** (and more axial compressed beta electron densities; see Figure S1, Supporting Information). It is interesting to observe that among the heteroleptic models $2H_2O/6OH^-$ matches not only the axiality but also the orientation of the magnetic moment of **3** with an angle between the two vectors of only 4°, while $5H_2O/3OH^-$ is deviated 45°. This fact is related with the delocalization of the negative charge on the carboxylate groups in acac ligands, which is better represented by two negatively charged equivalent groups (i.e., two OH^-) than with a neutral and negatively charged couple (one H_2O and one OH^-).

In order to verify the role of the metal−ligand electron repulsion, we employed DFT calculations of the ligand environment by excluding the Dy^{III} center by means of which we constructed electrostatic potential maps of the coordinated ligands at the Dy position. As shown in Figure 3, the homoleptic models presented almost isotropic electrostatic potentials, thereby confirming the lack of a preferential orientation for the electron density of the Dy^{III} centers and consequently the lack of magnetic anisotropy. For the heteroleptic systems combining water and OH^- ligands, the regions closer to the water ligands presented a less negative electrostatic potential (blue regions in Figure 3). Thus, the high and low islands of the electrostatic potential are located on opposite sides of the sphere. In such cases, the metal beta electron density is located between them in the direction of the minimum electrostatic potential of the sphere (blue regions in Figure 3 for complexes with H_2O and OH^- ligands simultaneously), thereby averting proximity with the more negatively charged ligands (for complexes with similar coordinated atoms to the metal, the shortest metal-ligand distance will determine the orientation of the magnetic moment). Finally, it is worth bearing in mind that the magnetic anisotropy axis will be perpendicular to the disc.

With this very intuitive idea we return to Figure 1 and look for the plane containing the ligands that results in the lowest electrostatic potential, and we can predict that the magnetization easy axis is perpendicular to that plane. This of kind of analysis could be particularly useful in polynuclear complexes where the relative orientations of the local magnetization easy axis could be predicted despite the fact that small variations on the real systems could modify the magnetic properties, as discussed in the Introduction. Also, it is worth mentioning that differences in first coordination sphere distances can significantly modify the role of the electrostatic potential of the ligands. Recently, publication of the polynuclear Dy_4 complex showing a barrier larger than 800 K because relaxation through the first excited state is quenched since it has a very similar magnetization to the ground state is noteworthy.[50] Thus, this fact shows that relaxation occurs through the next excited state leading to the large energy barrier. Dy^{III} centers adopt an octahedral coordination with ligands with different charges (five alkoxido and one oxo groups) that promote anisotropy in agreement with our predictions. This situation was not detected in any of the studied complexes in this paper that have larger coordination numbers.

Electrostatic potential maps were also constructed for complete structures of the systems for which we performed the calculations (Figure S2, Supporting Information). We observed that several systems presented a similar electrostatic potential shape, with a small less negative region originated by

dx.doi.org/10.1021/ic402367c | Inorg. Chem. 2013, 52, 13770−13778

the neutral ligands (in most cases bipyridine) and a more repulsive environment closer to the negative ligands, as in the heteroleptic models of **3**. Some other structures (the sandwich moieties of **9**, **10**, **18**, and **19** and the trigonal prismatic YACYOS complex, **21**) present two high-potential islands in opposite regions of the sphere, with a low potential in the equatorial region because of their shapes. In such cases, the beta electron density is accommodated in the equatorial region, thereby leading to the relatively low g_z values of the sandwiched complexes (around 16, see Table 1) and a beta electron density that loses its disc shape, similar that proposed by Rinehart et al.[22] for an $m_J = 13/2$ ground state.

Finally, we analyzed the nine-coordinated $[Dy(DOTA)(H_2O)]^-$ complex reported by Sessoli and co-workers;[26] their calculations predicted an extremely large dependence of its magnetic properties with the position of the hydrogen atoms of the water ligand. We employed three model structures in our calculations (two models with the hydrogen atoms of water molecule as placed expected just differing by a 30° rotation and the third one with the two water hydrogen atoms and the O−Dy bond lying in the same plane). Calculated g tensor components for the three models show a large dependence with the variation of the hydrogen atoms, in agreement with the original study (Table S4, Supporting Information). We notice that the pattern of spin-free excitation energies is similar for the three models, with a ground state and two low-lying excited states that are close in energy. It is worth remarking that such pattern is different from that found in the previously studied complexes (see Table S2, Supporting Information). Hence, the spin−orbit-coupled ground state will be a mixture of the ground spin-free level with the two excited states, with the relative weight of these excited states being highly dependent on small differences between them resulting in the large dependence found with the hydrogen positions. The electrostatic potential of the ligands presents a large low-repulsive region, associated with the formally neutral nitrogen atoms, and a high-potential zone pointing to the carboxylate groups. The variations on the hydrogen atoms of the axial water ligand have a clear effect on the electrostatic potential distribution (Figure S5, Supporting Information), while the plot of the spin-free beta electron density is less sensitive to such changes (Figure S4, Supporting Information). Large changes in the state mixing (see differences in the calculated E_1 and E_2 values in Table S4, Supporting Information) will have an effect on the ground state after inclusion of spin−orbit coupling, resulting in a dramatic change of the magnetic behavior.

CONCLUSIONS

We studied the performance of the CASSCF+RASSI method when modeling the magnetic properties of a set of X-ray-determined Dy^{III} complexes exhibiting zero-field SMM, field-induced SMM, and no SMM behavior. We found that the axiality of the main components of the g tensor of the ground Kramers' doublet can be successfully related with the presence of slow relaxation of magnetization in a number of cases. However, first excitation energies could not be compared directly with effective demagnetization barriers. It can be stated that both triangular dodecahedron and square antiprismatic coordination geometries are suitable for SMM behavior, while cubic coordination is less favorable for it. However, the nature of the ligands is crucial to the symmetry of the ligand field potential, and hence, it is difficult to analyze real systems in such terms, not only because of deviations from ideal geometries but also because of the presence of different ligands. Simple calculations based only on the position of the ligands in real systems can lead to different magnetic properties from those of the full system, especially if differences in the ligand charges are not taken into account. From calculations of model systems with ligands with different charge distributions we conclude that the high anisotropy of the ligand electrostatic potential related with heteroleptic systems favors SMM behavior, while more isotropy (homoleptic cases) prevents it. Almost all zero-field SMMs presented an electrostatic potential with a similar shape, with one low-electrostatic potential island near the neutral ligands within a high-potential region close to the anionic groups. In most real systems, the beta electron density of Dy^{III} f electrons (corresponding to the two beta 4f electrons) tends to concentrate into an axially compressed shape, similar to a disc, as expected for the $^6H_{15/2}$ $m_J = 15/2$ ground state. Furthermore, this electron density is accommodated toward the low electrostatic potential region caused by the ligand environment, thereby minimizing electron repulsion and hinting at the relation between the distribution of electrons in the Dy^{III} ion and the ligand position. Thus, it is possible to predict the direction of the magnetic anisotropy axis, which is perpendicular to the disc surface. Similar results were recently obtained by Chilton et al. using a simple electrostatic model with the charges of the atoms coordinated to the metal center to predict the orientation of the magnetic moment.[51] Consequently, in order to promote SMM behavior in Dy^{III} complexes, charged ligands should be combined with neutral ligands that provide a low-potential region in order to "pin" the electron distribution of the Dy^{III} center in a given orientation, promoting magnetic anisotropy. A second family of systems consists of the sandwich complexes (or those with an equivalent ligand distribution) with two high-potential regions close to the ligands and an equatorial low-electrostatic potential region that is the most favorable place for the electron density of the Dy^{III} centers. Such complexes usually have lower magnetic anisotropy than the heteroleptic complexes, and the shape of the calculated electron density is in agreement with a $^6H_{15/2}$ $m_J = 13/2$ ground state. Finally, we show that our model can also justify the large dependence of the magnetic properties with the position of the hydrogen atoms in the previously reported $[Dy(DOTA)(H_2O)]^-$ anionic complex.

COMPUTATIONAL DETAILS

Spin−orbit-free states for mononuclear complexes consisting of one Dy^{III} cation surrounded by its ligand coordination sphere were obtained using the CASSCF method, and the effect of spin−orbit coupling was taken into account in a second step using the restricted active space state interaction method (RASSI). The MOLCAS ANO-RCC basis set was used for all atoms.[52] The following contractions were used: Dy [9s8p6d4f3g2h]; Si [5s4p3d2f]; O [4s3p1d]; N [4s3p1d]; S [4s3p1d]; F [3s2p]; C [3s2p]; Li [3s2p] and H [2s]. A (9,7) active space and 21 sextets, 128 quadruplets, and 98 doublets were used. The direction and magnitude of the magnetic moment of the final states were evaluated using the SINGLE_ANISO[53] routine implemented in MOLCAS 7.8.[52] Models for **6**, **7**, **13**, **14**, **19**, **20**, and **22** were truncated in order to allow for CASSCF calculations: in **13**, the anthracene groups were replaced by methyl groups; in **14** and **22**, the naphthyl and phenyl groups were changed for H atoms; in **17**, the bis(1,2-dimethoxyethane)potassium moieties on top of the annulene ligands were removed; in **6**, **7**, and **20**, the thien-2-yl substituents in the acac groups were replaced by H atoms. We repeated the calculations for **7** and **20** in the full models and found no differences in the main components of the g tensor or energies with respect to the truncated models. Electrostatic potentials of the ligand environment of

dx.doi.org/10.1021/ic402367c | Inorg. Chem. 2013, 52, 13770−13778

the complexes were calculated using DFT methodology using a model structure just eliminating the metal atom, employing the B3LYP functional[54] and the TZVP basis set,[55] by means of the Gaussian09 package.[56]

■ ASSOCIATED CONTENT

Supporting Information

Full name of the studied complexes; continuous symmetry measurements for the studied Dy^{III} complexes with coordination 8; calculated *g* components at the CASSCF level for some model complexes; electron density of the beta electrons of the first four spin-free states for some Dy^{III} complexes; electrostatic potential originated from the ligand environment for some Dy^{III} complexes; electron density of the beta electrons of the first four spin-free states for some sandwich-shape Dy^{III} complexes; calculated spin Hamiltonian parameters for the $[Dy(DOTA)(H_2O)]^-$ anionic complex, electron density of the beta electrons of the first four spin-free states for the $[Dy(DOTA)(H_2O)]^-$ complex; electrostatic potential originated from the ligand environment for the $[Dy(DOTA)(H_2O)]^-$ complex. This material is available free of charge via the Internet at http://pubs.acs.org.

■ AUTHOR INFORMATION

Corresponding Author

*E-mail: eliseo.ruiz@qi.ub.es.

Notes

The authors declare no competing financial interest.

■ ACKNOWLEDGMENTS

The research reported here was supported by the Spanish Ministerio de Economía y Competitividad (grants CTQ2011-23862-C02-01) and the regional Generalitat de Catalunya authority (2009SGR-1459). D.A. thanks to Conicyt-Chile for a predoctoral fellowship. The authors thankfully acknowledge the computer resources, technical expertise and assistance provided by the CESCA.

■ REFERENCES

(1) Sessoli, R.; Gatteschi, D.; Caneshi, A.; Novak, M. A. *Nature* **1993**, *365*, 141.
(2) Gatteschi, D.; Sessoli, R.; Villain, J. *Molecular Nanomagnets*; Oxford University Press: Oxford, 2006.
(3) Gatteschi, D.; Sessoli, R. *Angew. Chem., Int. Ed.* **2003**, *42*, 268.
(4) Friedman, J. R.; Sarachik, M. P. *Annu. Rev. Condens. Matter Phys.* **2010**, *1*, 109.
(5) Aromi, G.; Brechin, E. K. *Struct. Bonding (Berlin)* **2006**, *122*, 1.
(6) Aromí, G.; McInnes, E. J. L.; Winpenny, R. E. P. In *Molecular Cluster Magnets*; Winpenny, R., Ed.; World Scientific: Singapore, 2012.
(7) Ishikawa, N.; Sugita, M.; Ishikawa, T.; Koshihara, S.; Kaizu, Y. *J. Am. Chem. Soc.* **2003**, *125*, 8694.
(8) Woodruff, D. N.; Winpenny, R. E. P.; Layfield, R. A. *Chem. Rev.* **2013**, *113*, 5110.
(9) Zhang, P.; Guo, Y.-N.; Tang, J. *Coord. Chem. Rev.* **2013**, *257*, 1728.
(10) Sessoli, R.; Powell, A. K. *Coord. Chem. Rev.* **2009**, *253*, 2328.
(11) Freedman, D. E.; Harman, W. H.; Harris, T. D.; Long, G. J.; Chang, C. J.; Long, J. R. *J. Am. Chem. Soc.* **2010**, *132*, 1224.
(12) Harman, W. H.; Harris, T. D.; Freedman, D. E.; Fong, H.; Chang, A.; Rinehart, J. D.; Ozarowski, A.; Sougrati, M. T.; Grandjean, F.; Long, G. J.; Long, J. R.; Chang, C. J. *J. Am. Chem. Soc.* **2010**, *132*, 18115.
(13) Zadrozny, J. M.; Atanasov, M.; Bryan, A. M.; Lin, C. Y.; Rekken, B. D.; Power, P. P.; Neese, F.; Long, J. R. *Chem. Sci.* **2013**, *4*, 125.
(14) Jurca, T.; Farghal, A.; Lin, P.-H.; Korobkov, I.; Murugesu, M.; Richeson, D. S. *J. Am. Chem. Soc.* **2011**, *133*, 15814.
(15) Gomez-Coca, S.; Cremades, E.; Aliaga-Alcalde, N.; Ruiz, E. *J. Am. Chem. Soc.* **2013**, *135*, 7010.
(16) Lin, P.-H.; Smythe, N. C.; Gorelsky, S. I.; Maguire, S.; Henson, N. J.; Korobkov, I.; Scott, B. L.; Gordon, J. C.; Baker, R. T.; Murugesu, M. *J. Am. Chem. Soc.* **2011**, *133*, 15806.
(17) Sorace, L.; Benelli, C.; Gatteschi, D. *Chem. Soc. Rev.* **2011**, *40*, 3092.
(18) Boulon, M.-E.; C., G.; Luzon, J.; Degl'innocenti, C.; Perfetti, M.; Bernot, K.; Calvez, G.; Caneschi, A.; Sessoli, R. *Angew. Chem., Int. Ed.* **2013**, *52*, 350.
(19) Cremades, E.; Ruiz, E. *Inorg. Chem.* **2011**, *50*, 4016.
(20) Cirera, J.; Ruiz, E.; Alvarez, S.; Neese, F.; Kortus, J. *Chem.—Eur. J.* **2009**, *15*, 4078.
(21) Atanasov, M.; Comba, P.; Helmle, S.; Müller, D.; Neese, F. *Inorg. Chem.* **2012**, *51*, 12324.
(22) Rinehart, J. D.; Long, J. R. *Chem. Sci.* **2011**, *2*, 2078.
(23) Chilton, N. F.; Langley, S. K.; Moubaraki, B.; Soncini, A.; Batten, S. R.; Murray, K. S. *Chem. Sci.* **2013**, *4*, 1719.
(24) Baldovi, J. J.; Borras-Almenar, J. J.; Clemente-Juan, J. M.; Coronado, E.; Gaita-Arino, A. *Dalton Trans.* **2012**, *41*, 13705.
(25) Baldovi, J. J.; Cardona-Serra, S.; Clemente-Juan, J. M.; Coronado, E.; Gaita-Arino, A.; Palii, A. *Inorg. Chem.* **2012**, *51*, 12565.
(26) Cucinotta, G.; Perfetti, M.; Luzon, J.; Etienne, M.; Car, P.-E.; Caneschi, A.; Calvez, G.; Bernot, K.; Sessoli, R. *Angew. Chem., Int. Ed.* **2012**, *51*, 1606.
(27) Bhunia, A.; Gamer, M. T.; Ungur, L.; Chibotaru, L. F.; Powell, A. K.; Lan, Y.; Roesky, P. W.; Menges, F.; Riehn, C.; Niedner-Schatteburg, G. *Inorg. Chem.* **2012**, *51*, 9589.
(28) Feltham, H. L. C.; Lan, Y.; Kloewer, F.; Ungur, L.; Chibotaru, L. F.; Powell, A. K.; Brooker, S. *Chem.—Eur. J.* **2011**, *17*, 4362.
(29) Ungur, L.; Chibotaru, L. F. *Phys. Chem. Chem. Phys.* **2011**, *13*, 20086.
(30) Chen, G.-J.; Guo, Y.-N.; Tian, J.-L.; Tang, J.; Gu, W.; Liu, X.; Yan, S.-P.; Cheng, P.; Liao, D.-Z. *Chem.—Eur. J.* **2012**, *18*, 2484.
(31) Jiang, S.-D.; Wang, B.-W.; Su, G.; Wang, Z.-M.; Gao, S. *Angew. Chem., Int. Ed.* **2010**, *49*, 7448.
(32) Chen, G.-J.; Gao, C.-Y.; Tian, J.-L.; Tang, J.; Gu, W.; Liu, X.; Yan, S.-P.; Liao, D.-Z.; Cheng, P. *Dalton Trans.* **2011**, *40*, 5579.
(33) Wang, H.; Wang, K.; Tao, J.; Jiang, J. *Chem. Commun.* **2012**, *48*, 2973.
(34) Bi, Y.; Guo, Y.-N.; Zhao, L.; Guo, Y.; Lin, S.-Y.; Jiang, S.-D.; Tang, J.; Wang, B.-W.; Gao, S. *Chem.—Eur. J.* **2011**, *17*, 12476.
(35) Li, D.-P.; Wang, T.-W.; Li, C.-H.; Liu, D.-S.; Li, Y.-Z.; You, X.-Z. *Chem. Commun.* **2010**, *46*, 2929.
(36) Le Roy, J. J.; Jeletic, M.; Gorelsky, S. I.; Korobkov, I.; Ungur, L.; Chibotaru, L. F.; Murugesu, M. *J. Am. Chem. Soc.* **2013**, *135*, 3502.
(37) Jeletic, M.; Lin, P.-H.; Le Roy, J. J.; Korobkov, I.; Gorelsky, S. I.; Murugesu, M. *J. Am. Chem. Soc.* **2011**, *133*, 19286.
(38) Menelaou, M.; Ouharrou, F.; Rodríguez, L.; Roubeau, O.; Teat, S. J.; Aliaga-Alcalde, N. *Chem.—Eur. J.* **2012**, *18*, 11545.
(39) Li, D.-P.; Zhang, X.-P.; Wang, T.-W.; Ma, B.-B.; Li, C.-H.; Li, Y.-Z.; You, X.-Z. *Chem. Commun.* **2011**, *47*, 6867.
(40) Ruiz, J.; Mota, A. J.; A., R.-D.; Silvia Titos, S.; Herrera, J. M.; Ruiz, E.; Cremades, E.; Costes, J. P.; Colacio, E. *Chem. Commun.* **2012**, *48*, 7916.
(41) Williams, U. J.; Mahoney, B. D.; DeGregorio, P. T.; Carroll, P. J.; Nakamaru-Ogiso, E.; Kikkawa, J. M.; Schelter, E. J. *Chem. Commun.* **2012**, *48*, 5593.
(42) Wang, Y.; Li, X.-L.; Wang, T.-W.; Song, Y.; You, X.-Z. *Inorg. Chem.* **2010**, *49*, 969.
(43) Meihaus, K. R.; Rinehart, J. D.; Long, J. R. *Inorg. Chem.* **2011**, *50*, 8484.
(44) Pointillart, F.; Le Gal, Y.; Golhen, S. p.; Cador, O.; Ouahab, L. *Chem.—Eur. J.* **2011**, *17*, 10397.
(45) Atanasov, M.; Zadrozny, J. M.; Long, J. R.; Neese, F. *Chem. Sci.* **2013**, *4*, 139.

(46) Chibotaru, L. F.; Ungur, L.; Aronica, C.; Elmoll, H.; Pilet, G.; Luneau, D. *J. Am. Chem. Soc.* **2008**, *130*, 12445.
(47) Feltham, H. L. C.; Lan, Y.; Klöwer, F.; Ungur, L.; Chibotaru, L. F.; Powell, A. K.; Brooker, S. *Chem.—Eur. J.* **2011**, *17*, 4362.
(48) Alvarez, S.; Alemany, P.; Casanova, D.; Cirera, J.; Llunell, M.; Avnir, D. *Coord. Chem. Rev.* **2005**, *249*, 1693.
(49) Llunell, M.; Casanova, D.; Cirera, J.; Alemany, P.; Alvarez, S. *Shape v. 2.0*; Universitat de Barcelona: Barcelona, 2010.
(50) Blagg, R. J.; Ungur, L.; Tuna, F.; Speak, J.; Comar, P.; Collison, D.; Wernsdorfer, W.; McInnes, E. J. L.; Chibotaru, L. F.; Winpenny, R. E. P. *Nat. Chem.* **2013**, *5*, 673.
(51) Chilton, N. F.; Collison, D.; McInnes, E. J. L.; Winpenny, R. E. P.; Soncini, A. *Nat. Commun.* **2013**, *4*, 2551.
(52) Aquilante, F.; De Vico, L.; Ferre, N.; Ghigo, G.; Malmqvist, P. A.; Neograd y, P.; Pedersen, T. B.; Pitonak, M.; Reiher, M.; Roos, B. O.; Serrano-Andres, L.; Urban, M.; Veryazov, V.; Lindh, R. *J. Comput. Chem.* **2010**, *31*, 224.
(53) Chibotaru, L. F.; Ungur, L. *J. Chem. Phys.* **2012**, *137*, 064112.
(54) Becke, A. D. *J. Chem. Phys.* **1993**, *98*, 5648.
(55) Schaefer, A.; Huber, C.; Ahlrichs, R. *J. Chem. Phys.* **1994**, *100*, 5829.
(56) Frisch, M. J.; Trucks, G. W.; Schlegel, H. B.; Scuseria, G. E.; Robb, M. A.; Cheeseman, J. R.; Scalmani, G.; Barone, V.; Mennucci, B.; Petersson, G. A.; Nakatsuji, H.; Caricato, M.; Li, X.; Hratchian, H. P.; Izmaylov, A. F.; Bloino, J.; Zheng, G.; Sonnenberg, J. L.; Hada, M.; Ehara, M.; Toyota, K.; Fukuda, R.; Hasegawa, J.; Ishida, M.; Nakajima, T.; Honda, Y.; Kitao, O.; Nakai, H.; Vreven, T.; Montgomery, J., J. A.; Peralta, J. E.; Ogliaro, F.; Bearpark, M.; Heyd, J. J.; Brothers, E.; Kudin, K. N.; Staroverov, V. N.; Kobayashi, R.; Normand, J.; Raghavachari, K.; Rendell, A.; Burant, J. C.; Iyengar, S. S.; Tomasi, J.; Cossi, M.; Rega, N.; Millam, N. J.; Klene, M.; Knox, J. E.; Cross, J. B.; Bakken, V.; Adamo, C.; Jaramillo, J.; Gomperts, R.; Stratmann, R. E.; Yazyev, O.; Austin, A. J.; Cammi, R.; Pomelli, C.; Ochterski, J. W.; Martin, R. L.; Morokuma, K.; Zakrzewski, V. G.; Voth, G. A.; Salvador, P.; Dannenberg, J. J.; Dapprich, S.; Daniels, A. D.; Farkas, Ö.; Foresman, J. B.; Ortiz, J. V.; Cioslowski, J.; Fox, D. J. *Gaussian09*; Gaussian: Wallingford, CT, 2009.